Sizing up protoplanetary disks

Trapman, L.

6 | Mass constraints for 15 protoplanetary disks from HD 1–0

M. Kama, L. Trapman, D. Fedele, S. Bruderer, M. R. Hogerheijde, A. Miotello, E. F. van Dishoeck, C. Clarke and E. A. Bergin, 2020, A&A, 634, 88

Abstract

Context: Hydrogen deuteride (HD) rotational line emission can provide reliable protoplanetary disk gas mass measurements, but it is difficult to observe and detections have been limited to three T-Tauri disks. No new data have been available since the *Herschel* Space Observatory mission ended in 2013.

Aims: We set out to obtain new disk gas mass constraints by analyzing upper limits on HD 1 – 0 emission in *Herschel*/PACS archival data from the DIGIT key program.

Methods: With a focus on the Herbig Ae/Be disks, whose stars are more luminous than T Tauris, we determine upper limits for HD in data previously analyzed for its line detections. Their significance is studied with a grid of models run with the DALI physical-chemical code, customized to include deuterium chemistry.

Results: Nearly all the disks are constrained to $M_{\rm gas} \leq 0.1\,{\rm M}_{\odot}$, ruling out global gravitational instability. A strong constraint is obtained for the HD 163296 disk mass, $M_{\rm gas} \leq 0.067\,{\rm M}_{\odot}$, implying $\Delta_{\rm gd} \leq 100$. This HD-based mass limit is towards the low end of CO-based mass estimates for the disk, highlighting the large uncertainty in using only CO and suggesting that gas-phase CO depletion in HD 163296 is at most a factor of a few. The $M_{\rm gas}$ limits for HD 163296 and HD 100546, both bright disks with massive candidate protoplanetary systems, suggest disk-to-planet mass conversion efficiencies of $M_{\rm p}/(M_{\rm gas}+M_{\rm p}) \approx 10$ to 40 % for present-day values. Near-future observations with SOFIA/HIRMES will be able to detect HD in the brightest Herbig Ae/Be disks within 150 pc with ≈ 10 h integration time.

6.1 Introduction

The elusive total gas mass of a protoplanetary disk is relevant for planet formation, dust dynamics, and for testing disk evolution models. Due to difficulties in observing H_2, $M_{\rm gas}$ has been robustly measured in only three cases. In this work, we use *Herschel* archival data to constrain $M_{\rm gas}$ in a sample of 15 Herbig Ae/Be disks, and determine the mass of HD 163296 to within a factor of a few.

The gas mass is dominated by H_2, which has a large energy spacing between its lowest rotational levels (*para*-H_2 $J = 2-0$, $\Delta E = 512\,$K) and lacks a dipole moment. As such, H_2 is not emissive at the 10-100 K temperatures typical for disks. Dust continuum emission at millimeter wavelengths is often used to estimate $M_{\rm gas}$. Gas and dust are linked through a mass ratio, canonically $\Delta_{\rm gd} = 100$ for solar-composition material below $\sim 10^3$ K (e.g. Lodders 2003). While dust emission is easy to detect, the different dust and gas evolution as well as uncertain opacity values limit its reliability in measuring $M_{\rm gas}$. The most precise $M_{\rm gas}$ measurements to-date are from hydrogen deuteride (HD) rotational lines. The relative abundance of this deuterated isotopolog of H_2 is set by the local absolute D-to-H ratio ($(2.0 \pm 0.1) \times 10^{-5}$, Prodanović et al. 2010) and minimally affected by disk chemistry (Trapman et al. 2017). As the $J = 1$ rotational level is at $E/k_B = 128.5\,$K, HD emits from warm gas ($T_{\rm gas} \approx 30$ to 50 K, Bergin et al. 2013; Trapman et al. 2017). This is sufficient to constrain the total $M_{\rm gas}$, especially if the temperature structure is constrained via other observables. The HD $J = 1-0$ line at $112\,\mu$m, is however impossible to observe from the ground due to atmospheric absorption and requires air- or spaceborne telescopes.

After the pioneering HD $1-0$ detection in TW Hya (Bergin et al. 2013; Trapman et al. 2017), facilitated by the PACS spectrometer (Poglitsch et al. 2010b) on the *Herschel Space Observatory* (Pilbratt et al. 2010b), further detections were only made in DM Tau and GM Aur (McClure et al. 2016) before the instrument expired. The masses of these T Tauri disks are $M_{\rm gas} = (6-9) \times 10^{-3}$, $(1-4.7) \times 10^{-2}$, and $(2.5-20.4) \times 10^{-2}\,{\rm M}_\odot$, respectively. An upper limit $M_{\rm gas} \leq 8 \times 10^{-2}\,{\rm M}_\odot$ was obtained for the Herbig Ae/Be system HD 100546 (Kama et al. 2016b, revised down from the published value due to a mistake in the D/H ratio).

In this work, we use the 2D physical-chemical code `DALI` (Bruderer et al. 2012; Bruderer 2013) to constrain $M_{\rm gas}$ in 15 disks by analyzing *Herschel* archival data covering the HD $1-0$ and $2-1$ lines. The data and models are discussed in Sections 6.2 and 6.3, respectively. In Section 6.4, we explore the disk mass constraints, with a focus on HD 163296, and discuss the potential for gravitational instability. In Section 6.5, we compare the mass of disks, stars, and planetary systems for stars over $1.4\,{\rm M}_\odot$. We also discuss future observations of HD with SOFIA/HIRMES (Richards et al. 2018) and SPICA/SAFARI (Nakagawa et al. 2014; Audley et al. 2018).

6.2 Observations and sample

We use archival data from the *Herschel Space Observatory* (Pilbratt et al. 2010b) key program DIGIT (PI N.J. Evans), which targeted 30 protoplanetary disks with the PACS (Poglitsch et al. 2010b) instrument at 50–210 μm. Detected gaseous species in this data were presented in Fedele et al. (2013) and Meeus et al. (2013). We analyze upper limits on HD $J = 1-0$ and $2-1$ lines at 112 and 56 μm for the 15 Herbig Ae/Be

disks in the sample. Due to the intrinsically higher luminosity of their host stars (~ 10-$100\,L_\odot$), these disks are warmer, and brighter in continuum and line emission than those around T Tauri stars. This enables tighter constraints for disks at equivalent distance.

Table 6.1: HD line flux upper limits (3σ) for the sample.

Name	$L_\star$ ($L_\odot$)	$T_{\rm eff}$ (K)	d (pc)	HD 112 μm ($10^{-17}\frac{W}{m^2}$)	HD 56 μm ($10^{-17}\frac{W}{m^2}$)	$F_{1.3\rm mm}$ (mJy)	Meeus group
HD 104237	$26^{\rm F15}$	$8000^{\rm F15}$	$108^{\rm GDR2}$	≤ 0.9	≤ 2.4	$92 \pm 19^{\rm M14}$	IIa
HD 144668	$58^{\rm F15}$	$8500^{\rm F15}$	$161^{\rm GDR2}$	≤ 0.8	≤ 7.8	$20 \pm 16^{\rm M14}$	IIa
HD 163296	$31^{\rm F12}$	$9200^{\rm F12}$	$101^{\rm GDR2}$	≤ 0.6	≤ 3.0	$743 \pm 15^{\rm M14}$	IIa
HD 31293	$59^{\rm F15}$	$9800^{\rm F12}$	$139^{\rm F12}$	≤ 4.2	≤ 22.4	$136 \pm 15^{\rm M14}$	Ia
HD 36112	$22^{\rm M14}$	$8190^{\rm F12}$	$160^{\rm GDR2}$	≤ 0.6	≤ 7.6	$72 \pm 13^{\rm M14}$	Ia
HD 38120	$123^{\rm S13}$	$10471^{\rm S13}$	$406^{\rm GDR2}$	≤ 0.9	≤ 5.6	-	Ia
HD 100546	$36^{\rm K16b}$	$10390^{\rm K16b}$	$110^{\rm GDR2}$	≤ 2.7	≤ 16.0	$465 \pm 20^{\rm M14}$	Ia
HD 139614	$6.6^{\rm F15}$	$7750^{\rm F15}$	$135^{\rm GDR2}$	≤ 1.2	≤ 8.5	$242 \pm 15^{\rm M14}$	Ia
HD 142527	$7.9^{\rm F15}$	$6500^{\rm F15}$	$157^{\rm GDR2}$	≤ 4.0	≤ 13.0	$1190 \pm 33^{\rm M14}$	Ia
HD 179218	$110^{\rm F12}$	$9640^{\rm F12}$	$266^{\rm GDR2}$	≤ 1.1	≤ 7.0	$71 \pm 7^{\rm M14}$	Ia
HD 97048	$33^{\rm F15}$	$10500^{\rm F15}$	$171^{\rm F15}$	≤ 2.4	≤ 2.4	$454 \pm 34^{\rm M14}$	Ib
HD 100453	$8.5^{\rm F15}$	$7250^{\rm F15}$	$104^{\rm GDR2}$	≤ 1.3	≤ 5.5	$200 \pm 21^{\rm M14}$	Ib
HD 135344B	$7.1^{\rm F15}$	$6375^{\rm F15}$	$136^{\rm GDR2}$	≤ 0.6	≤ 8.2	$142 \pm 19^{\rm M14}$	Ib
HD 169142	$10^{\rm F12}$	$7500^{\rm F12}$	$114^{\rm GDR2}$	≤ 2.4	≤ 13.5	$197 \pm 15^{\rm M14}$	Ib
Oph IRS 48*	$14.3^{\rm S13}$	$9000^{\rm S13}$	$134^{\rm GDR2}$	≤ 1.2	≤ 8.3	$60 \pm 10^{\rm M14}$	Ib

Notes. * – WLY 2-48.
References: F12 – Folsom et al. (2012); S13 – Salyk et al. (2013); M14 – Maaskant et al. (2014) and references therein; F15 – Fairlamb et al. (2015); K16b – Kama et al. (2016b); GDR2 – Brown et al. (2018).

We selected disks around stars of spectral type mid-F to late-B, including well-known targets such as HD 100546 and HD 163296. HD 50138 was excluded as it is likely an evolved star (Ellerbroek et al. 2015), and HD 35187 because it is a binary of two intermediate-mass stars and not directly comparable to our model grid. The data are spectrally unresolved, with $\delta v \approx 100\,{\rm km\,s^{-1}}$ ($\lambda/\delta\lambda = 3000$) at the shortest

wavelengths (51 μm), while expected linewidths are $\leq$ 10 km s^{-1}. Exposure times ranged from 4356 s to 8884 s. The system parameters and 3σ line flux upper limits are given in Table 6.1.

We obtained flux limits for the HD transitions from the 1σ noise reported for the nearest lines of other molecules from Fedele et al. (2013): OH $^2\Pi_{1/2}$ $J = 9/2^-$–$7/2^+$ at 55.89 μm for the 56 μm line and OH $^2\Pi_{3/2}$ $J = 5/2^-$–$3/2^+$ at 119.23 μm for the 112 μm line. With a typical 1σ uncertainty of 5×10^{-18} W m^{-2} at 112 μm and 2×10^{-17}W m^{-2} at 56 μm, neither of the HD lines is detected in the targets, individually or stacked. For comparison, the HD 1 – 0 detections Bergin et al. (2013) and McClure et al. (2016) had respective uncertainties of roughly 7×10^{-19} W m^{-2} and 5×10^{-19} W m^{-2}, which illustrates the difference between those targeted, deep integrations and the survey-type observations analyzed here.

The disks fall into two categories, cold (flat, group II in the Meeus classification, Meeus et al. 2001) and warm (flaring, group I). This characterizes the shape of the radial optically thick surface, where starlight is effectively absorbed. Starlight impinges at a shallow angle on flat disks, and heating is inefficient compared to that above the same midplane location in a flaring disk. In addition, among the Herbig Ae/Be systems flaring, group I disks have resolved cavities or gaps 10–100 au scales in their millimeter dust emission (Maaskant et al. 2013; Kama et al. 2015).

6.3 Modeling

6.3.1 DALI

To determine the behavior of the HD 1 – 0 line and 1.3 millimeter continuum flux as a function of disk structure parameters, we run a grid of models with the 2D physical-chemical disk code DALI (Bruderer et al. 2012; Bruderer 2013). The surface density is parameterized following the viscous accretion disk formalism (Lynden-Bell & Pringle 1974; Hartmann et al. 1998):

$$\Sigma_{\rm gas} = \Sigma_c \left(\frac{R}{R_c}\right)^{\gamma} \exp\left[-\left(\frac{R}{R_c}\right)^{2-\gamma}\right], \tag{6.1}$$

where Σ_c is the surface density at the characteristic radius R_c, and γ the power-law index which is generally 1. Assuming an isothermal structure in hydrostatic equilibrium, the vertical structure is given by a Gaussian density distribution (Kenyon & Hartmann 1987):

$$\rho_{\rm gas}(R,z) = \frac{\Sigma_{\rm gas}(R)}{\sqrt{2\pi}Rh} \exp\left[-\frac{1}{2}\left(\frac{z}{Rh}\right)^2\right]. \tag{6.2}$$

Here $h = h_c(R/R_c)^{\psi}$, ψ is the flaring index and h_c is the disk opening angle at R_c.

A population of small grains (0.005-1 μm), with a mass fraction $f_{\rm small}$, follows the gas density distribution given in Eq. (6.2). A second population, consisting of large grains (1 μm - 1 mm), has a mass fraction $f_{\rm large}$. Their scale height is χh, where $\chi \in (0, 1]$ is the settling parameter.

Table 6.2: `DALI` model grid parameters.

Parameter	Range
Chemistry	
Chemical age	1 Myr
HD/H_2	$4 \cdot 10^{-5}$
Physical structure	
γ	1.0
ψ	[0.0, 0.3]
h_c	[0.05, 0.15] rad
R_c	[50, 150] au
M_{gas}	$[10^{-3}, 10^{-2}, 10^{-1}]$ $M_\odot$
Dust properties	
Gas-to-dust ratio	[10, 50, 100, 300]
f_{large}	[0.8, 0.95]
χ	[0.2, 0.5]
f_{PAH}	0.001
Stellar properties[1]	
T_{eff}	10390 K
L_X	$8{\cdot}10^{28}$ erg s^{-1}
T_X	$7{\cdot}10^7$ K
L_*	[10, 50, 115] $L_\odot$
ζ_{cr}	10^{-17} s^{-1}
Observational geometry	
i	60°
d	150 pc

Notes. Standard `DALI` parameter names as in Bruderer et al. (2012). Deuterium abundance from Prodanović et al. (2010).[1]HD 100546 (Bruderer et al. 2012).

For the dust opacities of both small and large grain populations we assume a standard interstellar composition following Weingartner & Draine (2001), in line with Bruderer (2013). The absorption coefficient for the small (large) grains is $29.9\,cm^2\,g^{-1}$ ($30.0\,cm^2\,g^{-1}$) at $112\,\mu m$ and $154\,cm^2\,g^{-1}$ ($46.3\,cm^2\,g^{-1}$) at $56\,\mu m$.

First, the radiation field and dust temperature are determined from Monte Carlo radiative transfer. Next, the gas temperature (heating-cooling balance) and chemical composition (steady-state) are solved for iteratively. Raytracing then yields simulated line and continuum observations.

HD chemical network *versus* fixed abundance

The HD abundance (HD/H_2) can be prescribed as a constant or obtained from solving a chemical reaction network. In the parametric approach, the HD abundance is determined by the local D/H ratio, which for the local ISM (within $\approx 2\,kpc$) is measured to be $(D/H)_{ISM} = (2.0 \pm 0.1) \times 10^{-5}$ (Prodanović et al. 2010). Assuming all deuterium is in HD, this gives $HD/H_2 = 4 \times 10^{-5}$.

A more refined approach is to calculate the HD abundance using a reaction network which includes deuterium. Trapman et al. (2017) extended the standard DALI chemi-

cal network (originally based on the UMIST06 database Woodall et al. 2007) to include the species HD, D, HD^+, and D^+. HD formation on dust and ion-exchange reactions were included, in addition to HD self-shielding. The details of the implementation are described in Section 2.3 of Trapman et al. (2017).

Using the chemical network approach, we find that all of the available deuterium is locked up in HD for the vast majority of the disk, and the parametric abundance of $HD/H_2 = 4 \times 10^{-5}$ is appropriate to use. The network produces less HD in only two regions: the uppermost layers of the disk where HD is photodissociated, and in a thin intermediate layer, where the HD abundance is decreased by a factor of ~ 2. Tests determined that neither of these significantly affects the disk-integrated HD line flux.

Given the very close match between the two approaches, we opt for simplicity and fix the HD/H_2 ratio at 4×10^{-5}.

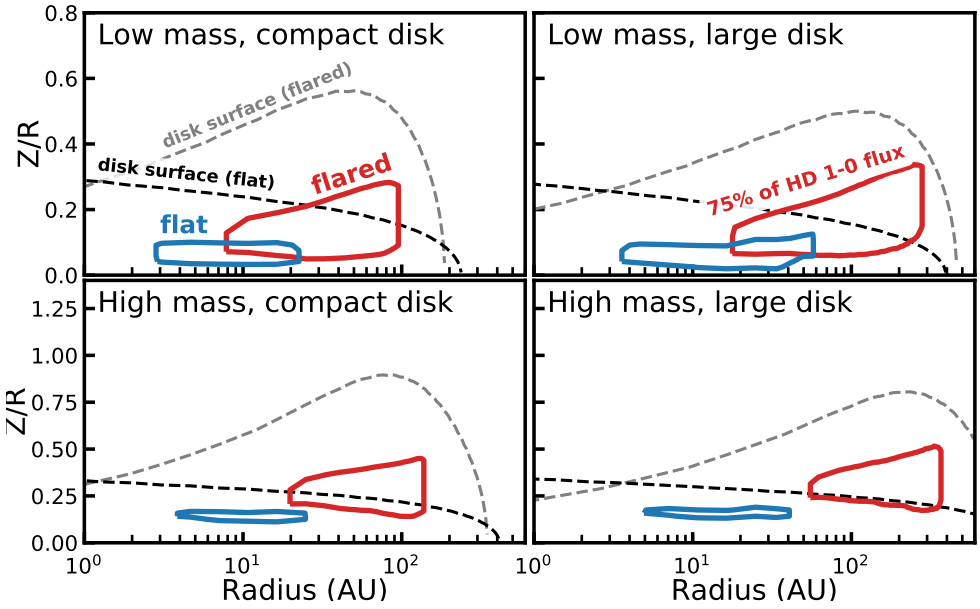

Figure 6.1: HD 1–0 line emitting regions in our flat/cold (blue) and flared/warm (red) disk models. Solid contours contain the middle 75% of vertically cumulative line emission. Dashed lines are gas number density iso-contours for $n_{\rm gas} = 10^6$ cm^{-3}, acting as a disk "outline".

6.3.2 Model grid

To investigate the range of disk properties constrained by the *Herschel* upper limits on the HD 1 – 0 line, we run a grid of Herbig Ae/Be disk models covering a wide range of parameters, summarized in Table 6.2. The disk gas masses are $M_{\rm gas} = 10^{-3}$, 10^{-2}, and $10^{-1}\,{\rm M}_\odot$. Dust mass is defined by the gas-to-dust mass ratio, with values $\Delta_{\rm gd} = 10$, 50, 100, and 300, and ranges from $M_{\rm dust} = 3 \times 10^{-6}$ to $10^{-2}\,{\rm M}_\odot$. The shape of the stellar spectrum, including UV excess, is based on HD 100564 from Bruderer et al. (2012). The spectrum is scaled to the total stellar luminosity, $L_\star \in [10, 50, 115]\,{\rm L}_\odot$. This covers the sources in our sample, as given in Table 6.1. In total we run 2304 models,

with parameters given in Table 6.2. Our fiducial model has $h_c = 0.15$, $R_c = 50\,\mathrm{au}$, $\Delta_{\mathrm{gd}} = 100$, $f_{\mathrm{large}} = 0.95$, $\chi = 0.2$, and $L_\star = 10\,\mathrm{L}_\odot$.

Figure 6.1 shows the HD 1 – 0 emitting regions and disk mass outline for models representing extremes in flaring ($\Psi = 0.0$ and $h_{\mathrm{c}} = 0.05$ for flat, and $\Psi = 0.3$ and $h_{\mathrm{c}} = 0.15$ for flared), radial extent ($R_{\mathrm{c}} = 50$ and $125\,\mathrm{au}$), and total disk mass. From the figure it is clear that the flared disk ($\psi = 0.3, h_c = 0.15$), shown in red, has a much large emitting region than the flat disk ($\Psi = 0.0, h_c = 0.05$), shown in blue. In both cases the HD 1 – 0 emission originates from the warm layer above the midplane.

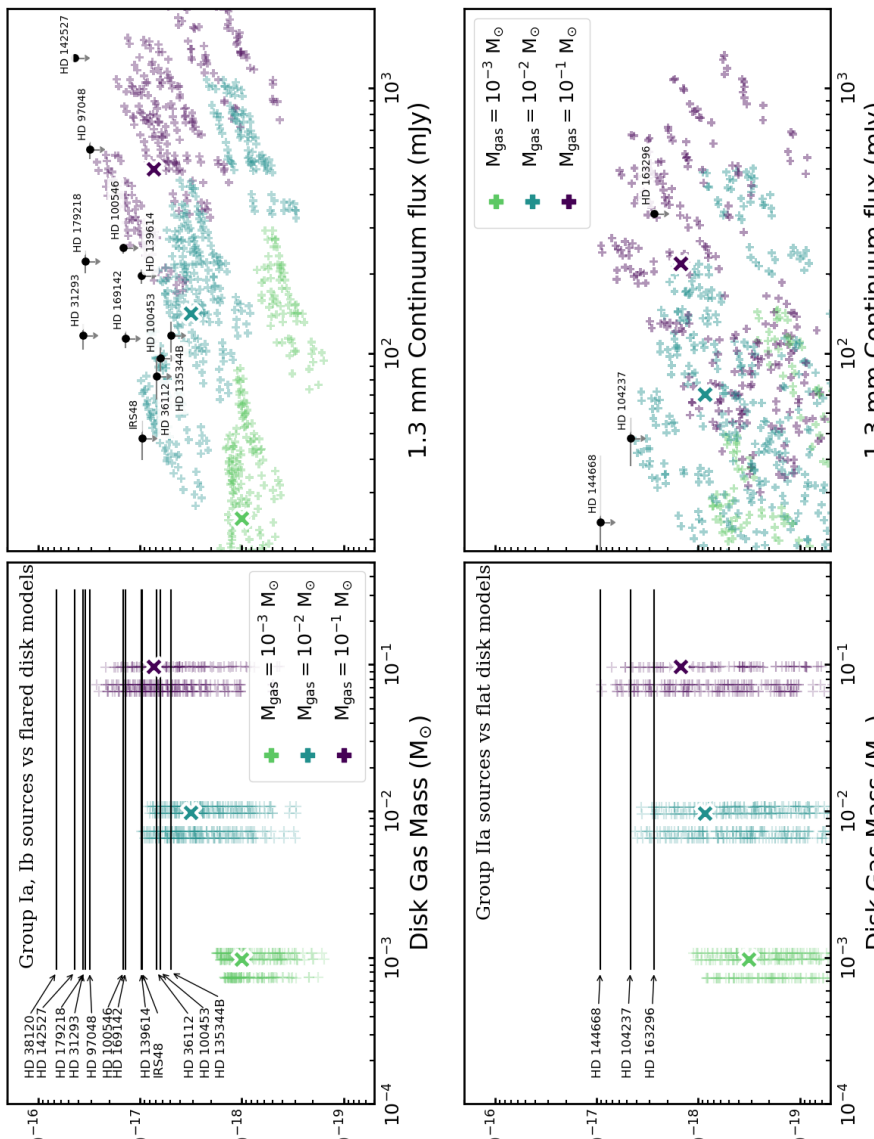

Figure 6.3:
Distance-normalized 3σ upper limits on HD 112 μm line flux for the disk sample (black lines and circles) compared with our grid of DALI disk models (colored crosses). Highlighted crosses show the HD 112 μm line flux of our fiducial model. The top panels show the group I sources compared to models with flaring angle $\psi = 0.3$. The bottom panels show the group II sources compared to models with $\psi = 0.0$. **Left:** models are separated based on gas mass. **Right:** HD 1 – 0 upper limits set against 1.3 mm continuum fluxes for both observations and models.

6.4 Results

In Figure 6.3, we show the HD $J = 1\text{-}0$ flux as a function of $M_{\rm gas}$ and 1.3 millimeter continuum flux. The warm, flaring, group I disks and cold, flat, group II disks are highlighted separately for clarity.

6.4.1 Parameter dependencies in the grid

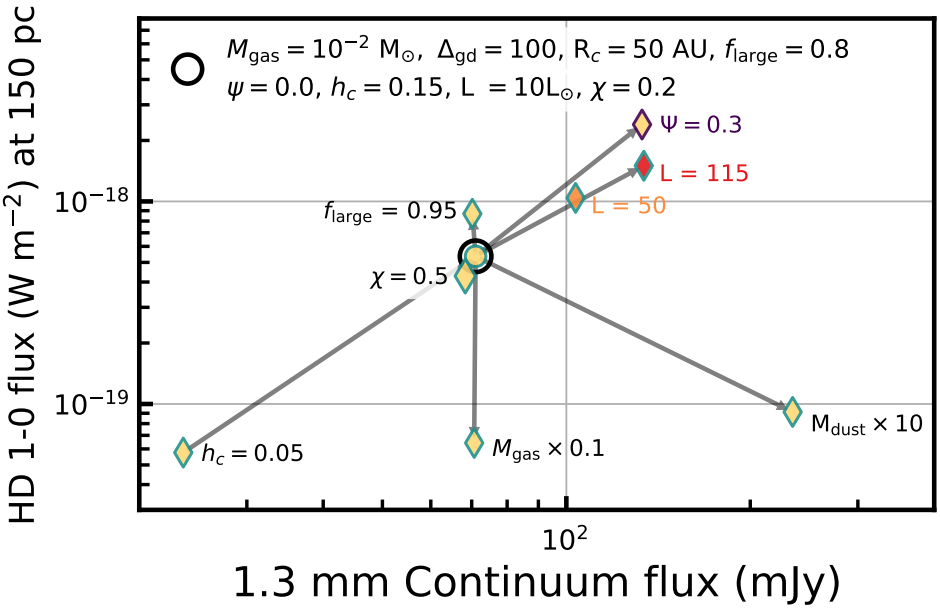

Figure 6.4: HD 1 – 0 line and dust continuum flux dependencies on disk and stellar parameters.

Dependencies of the HD 1 – 0 line and 1.3 millimeter continuum flux on the main model parameters are shown in Figure 6.4. The HD line flux depends linearly on $M_{\rm gas}$, which has only a marginal effect on the dust emission. For a fixed $M_{\rm gas}$, a 1 dex increase in $M_{\rm dust}$ leads to a factor 6.7 lower HD and 2.5 higher continuum flux. The flaring structure of the disk has the largest influence, as the HD line flux increases by a factor of 26 when the flaring parameter Ψ goes from 0 (height is linear with radius, inefficient heating) to 0.3 (very flared and efficiently heated). The Meeus group corresponds to the flaring structure (group I disks are flared, II flat).

A near-linear dependence of HD line flux on $M_{\rm gas}$ arises because the HD line emission in the models is vertically limited by the dust optical depth τ at 112 μm out to $\approx$ 100 au radii, beyond which the surface density drops rapidly. Thus the HD contribution from the gas above and radially outside the dust scales linearly with the total gas mass. Dust emission, to first order, is optically thin at 1.3 mm, and thus scales linearly with the total dust mass. Again due to the dust optical depth dominating at the 112 μm wavelength of HD 1 – 0, increasing the dust mass in a given column lifts

the vertical $\tau(112\,\mu\mathrm{m}) = 1$ surface, hiding a larger fraction of the HD molecules.

6.4.2 Constraints on M_{gas} across the sample

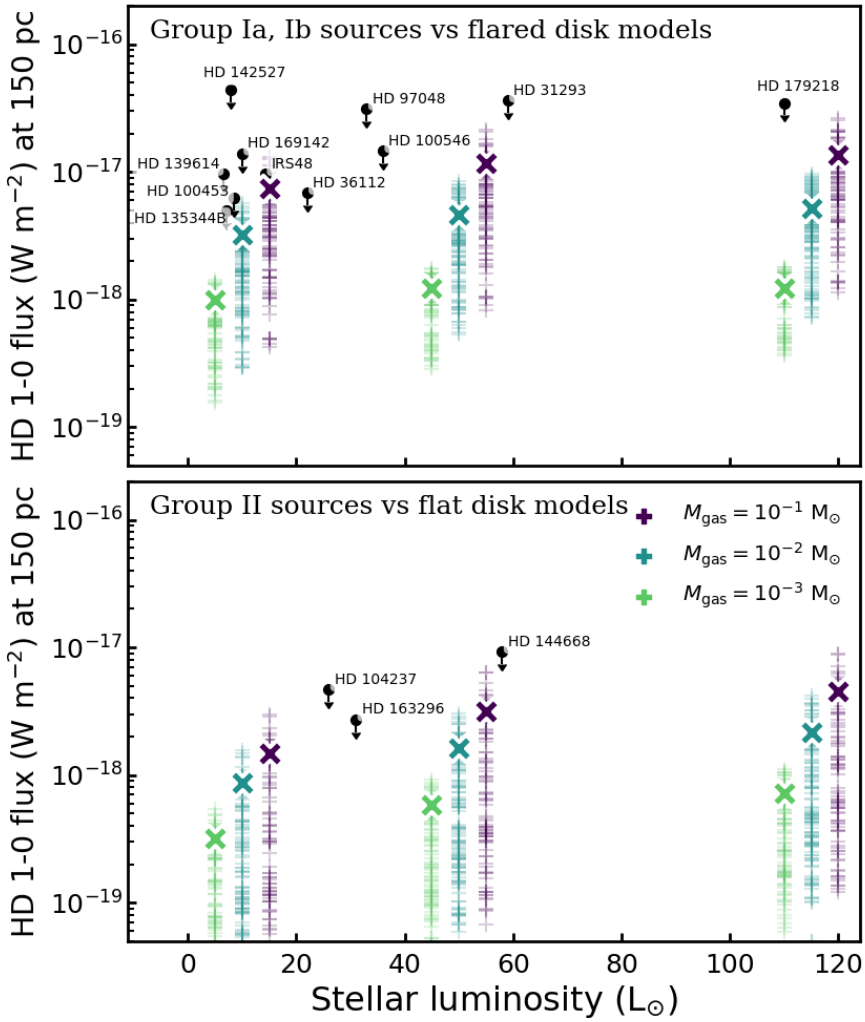

Figure 6.5: HD 1 – 0 line flux versus the stellar luminosity. Observed stellar luminosities taken from Table 6.1. Model stellar luminosities were given a small offset for clarity. Highlighted crosses show our fiducial model ($h_c = 0.15$, $R_c = 50\,\mathrm{au}$, $\Delta_{\mathrm{gd}} = 100$, $f_{\mathrm{large}} = 0.95$, $\chi = 0.2$).

A comparison of the HD upper limits from *Herschel* with our DALI model grid (Figures 6.3 and 6.5) places an upper limit of approximately $M_{\mathrm{gas}} \leq 0.1\,\mathrm{M}_\odot$ for the disks in our sample. Among the flared, group I disks (Fig. 6.3, upper row), we find $M_{\mathrm{gas}} < 0.02$–$0.03\,\mathrm{M}_\odot$ for IRS 48, HD 36112, HD 100453, and HD 135344B, while among the flat, group II disks HD 163296 has a limit at $< 0.1\,\mathrm{M}_\odot$.

Source-specific models can tighten the mass limit for individual disks. We run a small grid of models for HD 163296, where we have a strong HD upper limit and a wide comparison range of indirect gas mass estimates from the literature based on various isotopologs of CO.

6.4.3 HD 163296

We constrain the gas mass in the HD 163296 disk to $M_{\rm gas} \leq 0.067\,{\rm M}_\odot$ (Figure 6.6). Given that the disk-integrated dust mass in our model is $6.7 \times 10^{-4}\,{\rm M}_\odot$, this constrains the gas-to-dust ratio to $\Delta_{\rm gd} \leq 100$ and has implications for the gas-phase volatile abundances, which we discuss below. This source-specific model matches the continuum spectral energy distribution, ^{12}CO rotational ladder and isotopolog lines, and several other key volatile species. The full details of this modeling are outside the scope of this paper and will be published separately, below we focus on the main outcomes of the continuum, CO, and HD modeling.

Table 6.3: Adopted model for HD 163296

Parameter	Value
γ	0.9
ψ	0.05
$h_{\rm c}$	0.075
$R_{\rm c}$	125 au
$\Sigma_{\rm c}$ $R_{\rm cav}$	0.41 au
$M_{\rm gas}$	$6.7 \times 10^{-2}\,{\rm M}_\odot$
$M_{\rm dust}$	$6.6 \times 10^{-4}\,{\rm M}_\odot$
$\Delta_{\rm gd}$	100
$f_{\rm large}$	0.9
χ	0.2
L_* (L$_\odot$)	37.7
i (°)	45
d (pc)	101 pc

HD 163296 is one of the largest known disks, with a CO $J = 3-2$ gas emission radius of 540 au (Rosenfeld et al. 2013). Fitting of CO and 850 μm continuum emission, observed by ALMA, with a tapered surface density powerlaw yielded $\gamma = 0.9$ and $R_c = 125$ au (Tilling et al. 2012; de Gregorio-Monsalvo et al. 2013). We model HD 163296 with the stellar spectrum from the PRODiMo project (Woitke et al. 2019), fixing the shape of the dust surface density profile to the above parameters and varying the gas mass. To satisfy the radial profile of CO 3 – 2 emission simultaneously with the spectral energy distribution, we find the density profile flaring index in Eq. 6.2 is around $\psi = 0.05$, consistent with the range of 0.019 to 0.066 found by Tilling et al. (2012). The morphology of the ^{12}CO 3 – 2 channel maps, in which both the near and far side of the disk can be seen, suggest HD 163296 is more flared ($\psi \approx 0.12$, de Gregorio-Monsalvo et al. 2013) than our model ($\psi = 0.05$). However, these two ψ-s differ in physical meaning: the CO-based one measures the observed shape of the CO-emitting surface, while the disk structure parameter ψ characterizes the shape of the total gas mass distribution (see Eq. 6.2).

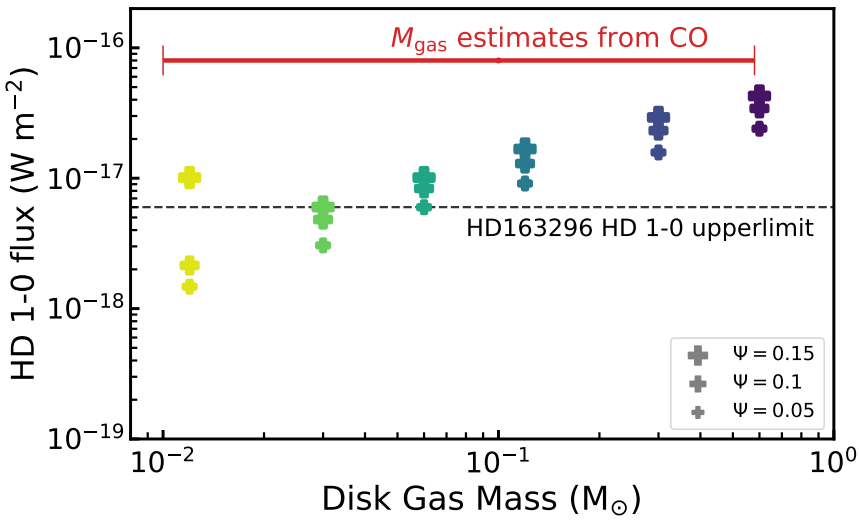

Figure 6.6: Comparing the HD 163296 specific models to the HD 1 − 0 upper limit (Fedele et al. 2013). All models have a dust mass $M_{\rm dust} = 6.6 \times 10^{-4}$ M$_\odot$ (Table 6.3). The red bar shows the range of gas masses inferred from CO in the literature.

Our model which hits the HD upper limit reproduces the observed dust emission across the far-infrared and sub-millimeter wavelengths as well as various spatially resolved and unresolved emission lines of ^{12}CO and its isotopologs, and has a gas-to-dust ratio $\Delta_{\rm gd} = 100$.

Most previous estimates of the HD 163296 gas mass relied on low-J emission lines of CO isotopologs, and used a range of modeling approaches from generic model grids to tailored modeling with physical-chemical codes. Those $M_{\rm gas}$ estimates range from 8×10^{-3} to 5.8×10^{-1} M$_\odot$ (Isella et al. 2007; Williams & Best 2014; Boneberg et al. 2016; Miotello et al. 2016; Williams & McPartland 2016; Powell et al. 2019; Woitke et al. 2019; Booth et al. 2019). The mass obtained from the most optically thin isotopolog among these, ^{13}C^{17}O, was 2.1×10^{-1}M$_\odot$ (Booth et al. 2019).

Above, we assumed an undepleted solar abundance for elemental gas-phase carbon and oxygen. Our model matching the HD upper limit over-produces the low-J line fluxes of CO isotopologs by a factor of a few. Since the rarer isotopologs are progressively more optically thin, we can reproduce their line fluxes by decreasing the gas-phase elemental carbon and oxygen abundance proportionately to the flux mismatch. Since the millimeter-wave dust emission and HD upper limit constrain the gas-to-dust mass ratio to be ≤ 100, we can combine the above considerations to arrive at three distinct hypotheses for HD 163296:

1. $M_{\rm gas}$ is just sufficiently below our upper limit of 6.7×10^{-2} M$_\odot$ for HD not to be detected. If so, then as the dust mass is fixed, it follows from our models that $\Delta_{\rm gd} = 100$ and that total gas-phase elemental C and O are depleted by up to a factor of a few.

2. $M_{\rm gas}$ is a factor of a few below our HD limit, and the total gas-phase elemental C and O abundances are not depleted with respect to their interstellar values.

If so, the implication is that $\Delta_{\rm gd} \approx 20$–$50$. This relative depletion of gas over dust is supported by the hydrostatic MCMax modeling of the SED and low-J ^{12}CO, ^{13}CO, and C^{18}O lines by Boneberg et al. (2016), whose best models had $9.2 < \Delta_{\rm gd} < 18$. It is also consistent with the inner disk value $\Delta_{\rm gd} \approx 55$, measured using accretion onto the central star by Kama et al. (2015, their Figure 2).

3. $M_{\rm gas}$ is far below our upper limit. In this hypothesis, the total C and O abundance in the gas must be enhanced above the interstellar baseline, in order to still match the optically thin CO isotopologs. This would be the first known case of C and O enhancement, however the inner disk composition analysis by Kama et al. (2015) does not show evidence for a strong enhancement of gas-phase volatile elements over total hydrogen.

Thus $\Delta_{\rm gd} > 100$ is ruled out by the HD $1-0$ upper limit for HD 163296, independently of assumptions about the precise abundance of gas-phase volatiles.

The abundance of volatile elements in the HD 163296 disk may be depleted or enhanced by up to a factor of a few, depending on the true value of $M_{\rm gas}$ and on the somewhat uncertain underlying number abundance ratios of ^{12}CO and its various isotopologs. We note that even with the flat, cold disk structure of HD 163296, our $\Delta_{\rm gd} = 100$ model somewhat over-predicts the CO emission outside of ~ 100 au for an undepleted elemental carbon abundance (C/H $= 1.35 \times 10^{-4}$). A more flared surface would aggravate this over-prediction, while globally reducing the elemental C under-predicts the CO $3-2$ inside ~ 100 au. This may indicate that any depletion of gas-phase volatile elemental C and O, reflected in the CO abundance in the warm molecular layer, is restricted to the region beyond the CO snowline, which has been observed to be at ≈ 90 au (Qi et al. 2015). The same conclusion was recently reached by Zhang et al. (2019) through an analysis of spatially resolved C^{18}O data, which yielded a factor of ten depletion of gas-phase CO outside the CO snowline.

6.4.4 HD 100546

HD 100546 was previously modeled with DALI by Bruderer et al. (2012) who determined the radial and vertical structure of the disk mainly from CO lines and continuum emission. A refined version of this modeling effort included the *Herschel* HD upper limits, the C^0 and C_2H fluxes, and the spatially resolved CO $3-2$ emission, constraining the gas mass to $8.1 \times 10^{-3} \leq M_{\rm gas} \leq 2.4 \times 10^{-1}\,{\rm M}_\odot$ (Kama et al. 2016b). The highest-mass model had $\Delta_{\rm gd} = 300$, with a dust mass anchored by the continuum spectral energy distribution. Due to a factor of four error in the D abundance used in that model, we revise those numbers to $\lesssim 100$ and thus $M_{\rm gas} \lesssim 0.08\,{\rm M}_\odot$ from the Kama et al. (2016b) model. This is about a factor of two stronger than the constraint from our general model grid, so in Figure 6.7 we adopt $M_{\rm gas} \lesssim 0.08\,{\rm M}_\odot$.

6.4.5 Other individual disks

HD 97048 hosts a massive dust disk, $M_{\rm dust} \simeq 6.7 \times 10^{-4}\,{\rm M}_\odot$ (Walsh et al. 2016), so it is likely the gas mass is also high. The disk surface is highly flared ($\Psi = 0.5 - 0.73$, see e.g. Lagage et al. 2006; Walsh et al. 2016; Ginski et al. 2016; van der Plas et al. 2019)). This exceeds the largest Ψ in our general grid, but we note again that the

CO-surface Ψ and the density structure Ψ differ in physical meaning. From our grid we find $M_{\rm gas} \leq 9.4 \cdot 10^{-2}\,{\rm M}_\odot$ ($\Delta_{\rm gd} \leq 200$).

HD 104237. For this disk, Hales et al. (2014) determined $M_{\rm dust} = 4 \times 10^{-4}\,{\rm M}_\odot$, which assuming $\Delta_{\rm gd} = 100$ implies a total mass $M_{\rm gas} = 4 \times 10^{-2}\,{\rm M}_\odot$. This is consistent with our upper limit from HD 1 – 0, which yields an upper limit of $\Delta_{\rm gd} \leq 300$ (Figure 6.3).

HD 36112 (MWC 758). Based on millimeter continuum interferometry, Guilloteau et al. (2011) inferred a disk mass of $(1.1 \pm 0.2) \times 10^{-2}\,{\rm M}_\odot$. Our analysis of the 1.3 mm continuum flux and the HD 1 – 0 upper limit matches both datapoints for $\Delta_{\rm gd} \approx 100$ and a disk mass of order $10^{-2}\,{\rm M}_\odot$. A substantially lower gas mass would imply a very low $\Delta_{\rm gd}$ mass ratio.

HD 31293 (AB Aurigae). From 1.3 millimeter continuum observations performed using the SMA, Andrews et al. (2013) inferred a dust mass of $(1.56 \pm 0.09) \times 10^{-4}\,{\rm M}_\odot$, implying $M_{\rm gas} = 1.56 \times 10^{-2}\,{\rm M}_\odot$ assuming $\Delta_{\rm gd}$= 100. The high upper limit of HD 1 - 0 for this source does not allow us to put any meaningful constraints on the gas mass based on HD.

HD 135344B has been modeled by van der Marel et al. (2016b) to determine the physical structure. Using ALMA observations of ^{13}CO $J = 3-2$, C^{18}O $J = 3-2$, ^{12}CO $J = 6-5$ and dust 690 GHz continuum, they determined a gas mass $M_{\rm gas} = 1.5 \times 10^{-2}\,{\rm M}_\odot$. We run models based on their physical structure and find the resulting HD 1 – 0 flux to be in agreement with the upper limit (see Figure 6.9 in Appendix 6.A).

HD 142527. Modeling interferometric 880 μm continuum and ^{13}CO 3–2 and C^{18}O 3–2 line observations, Boehler et al. (2017) determine a dust mass of $1.5 \times 10^{-3}\,{\rm M}_\odot$ and a gas mass of $5.7 \times 10^{-3}\,{\rm M}_\odot$ (see also Muto et al. 2015). This gives $3 \leq \Delta_{\rm gd} \leq 5$ and suggests the gas is either strongly depleted in elemental C and O, or dissipating entirely. Due to the loose HD 1 – 0 upper limit for this source, we cannot provide an independent check of the low $\Delta_{\rm gd}$ derived from CO.

HD 179218. From the integrated 1.3 millimeter flux Mannings & Sargent (2000) infer a dust mass of $(1.5 \pm 0.15) \times 10^{-4}\,{\rm M}_\odot$, implying $M_{\rm gas} = 1.5 \times 10^{-2}\,{\rm M}_\odot$ assuming $\Delta_{\rm gd}$= 100. Again the HD 1 – 0 upper limit provides no meaningful constraint on the gas mass.

HD 100453. Based on millimeter continuum interfermotric observations, van der Plas et al. (2019) inferred a dust mass of $6.7 \times 10^{-5}\,{\rm M}_\odot$. By comparing the ^{13}CO 2 – 1 and C^{18}O 2 – 1 to the disk model grid in Williams & Best (2014), they determine a gas mass of $(1 - 3\times) \times 10^{-3}\,{\rm M}_\odot$. Combining both disk masses implies a gas-to-dust mass ratio of $\Delta_{\rm gd}$ $15 - 45$. From our analysis of the 1.3 mm continuum flux and the HD 1 – 0 upper limit we constrain gas mass to $M_{\rm gas} \leq 10^{-2}\,{\rm M}_\odot$ and the gas-to-dust mass ratio $\Delta_{\rm gd} \leq 300$. Both constraints are in agreement with the results of van der Plas et al. (2019).

HD 169142. From interferometric 1.3 millimeter continuum and ^{12}CO 2 – 1, ^{13}CO 2 – 1 and C^{18}O 2 – 1 line observations, Panić et al. (2008) derived a dust mass of $2.16 \times 10^{-4}\,{\rm M}_\odot$ and a gas mass of $(0.6 - 3.0) \times 10^{-2}\,{\rm M}_\odot$. Fedele et al. (2017) find similar disk masses based on higher resolution observations. Constraints based on our analysis of the 1.3 mm continuum flux and the HD 1 – 0 upper limit put the gas mass at $M_{\rm gas} \leq 4 \times 10^{-2}\,{\rm M}_\odot$ and $\Delta_{\rm gd} \leq 300$, both of which are in good agreement with previous results.

Oph IRS 48 (WLY 2-48). van der Marel et al. (2016b) modeled the resolved 440 μm continuum and ^{13}CO 6 – 5 and C^{18}O 6 – 5 line observations. They derived a

dust mass of $1.5 \times 10^{-5}\,\mathrm{M}_\odot$ and a gas mass of $5.5 \times 10^{-4}\,\mathrm{M}_\odot$, giving a gas-to-dust mass ratio of $\Delta_{\mathrm{gd}} \approx 37$. Constraints from our analysis of the HD 1 – 0 line flux and 1.3 millimeter continuum give $M_{\mathrm{gas}} \lessapprox 10^{-2}\,\mathrm{M}_\odot$ and $\Delta_{\mathrm{gd}} \lessapprox 300$. These upper limits agree with previous results.

6.4.6 Are the disks stable?

Constraints on M_{gas} allow to test whether the disks in our sample are currently gravitationally stable. Gravitational instability, leading to spirals or fragmentation, occurs in disk regions which are dense and cold, and have low orbital shearing on the timescale of the instability (i.e. at large radii). This is quantified with the Toomre Q parameter, $Q = \Omega_K\, c_{\mathrm{s}}\, (\pi\, G\, \Sigma)^{-1}$ (Toomre 1964), which simplifies to

$$Q = 21 \times \left(\frac{\Sigma}{10\,\mathrm{kg\,m^{-2}}}\right)^{-1} \times \left(\frac{r}{100\,\mathrm{au}}\right)^{-3/2}, \tag{6.3}$$

following Kimura & Tsuribe (2012). If $Q < 1$, the disk will fragment. For $1 < Q < 2$, the disk will be marginally stable, developing transient spirals and clumps, while for $Q > 2$ it is stable against gravitational collapse. Assuming a surface density profile $\Sigma = \Sigma_0 \times (r/r_0)^{-1}$ and $M_{\mathrm{disk}} \approx M_{\mathrm{gas}}$, we obtain

$$Q = 2.44 \times 10^{22}\, \pi\, r_0^{1/2}\, M_{\mathrm{disk}}^{-1}, \tag{6.4}$$

Our most massive disk models have $M_{\mathrm{gas}} = 0.1\,\mathrm{M}_\odot$. Taking a characteristic radius $r_0 = 100\,\mathrm{au}$, we find $Q = 1.5$, which is marginally stable. The disks for which we have the weakest upper limits relative to the massive disk models – HD 142527, HD 144668, HD 179218, and HD 31293 – may potentially be gravitationally unstable within the limits of the *Herschel* HD data. For the rest of the sample, a gravitationally unstable M_{gas} is effectively ruled out, i.e. they are most likely stable.

6.5 Discussion

6.5.1 Mass of disks, stars, and planets

Intermediate-mass stars (spectral types B9 to F5, masses 1.5 to $3\,\mathrm{M}_\odot$) host some of the best-studied protoplanetary disks and high-mass planetary systems. Several Herbig Ae/Be protoplanetary disks have also yielded detections of protoplanet candidates. This presents an opportunity to investigate equivalent planetary systems at different stages of evolution. While radial velocity surveys

In Figure 6.7, we compare the disk mass reservoir with the host star and the mass of candidate protoplanets in the disk. We show two Herbig Ae/Be systems with strong mass limits, HD 163296 ($M_{\mathrm{gas}} \leq 0.067\,\mathrm{M}_\odot$, this work) and HD 100546 ($M_{\mathrm{gas}} \leq 0.08\,\mathrm{M}_\odot$, Kama et al. 2016b).

For HD 163296, our HD-based upper limit rules out a large fraction of the wide range of CO isotopolog based M_{gas} estimates from the literature. Of those still possible, the lowest is $M_{\mathrm{gas}} = 8 \times 10^{-3}\,\mathrm{M}_\odot$. The presence of five giant planets has been inferred from dust gaps and gas kinematics: at 10 au with a mass $(0.53 \pm 0.18)\,\mathrm{M_{Jup}}$ for $\alpha_{\mathrm{visc}} = 10^{-4}$ to 10^{-3} (Zhang et al. 2018); at 48 au with $0.46\,\mathrm{M_{Jup}}$ (Isella et al. 2016; Liu et al. 2018); at 86 au with $(1 \pm 0.5)\,\mathrm{M_{Jup}}$ (Liu et al. 2018; Teague et al.

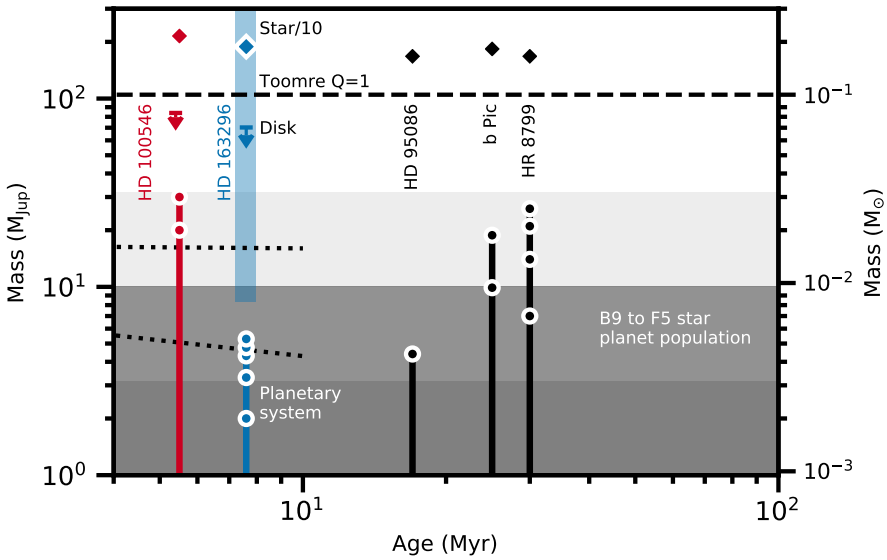

Figure 6.7: Mass of selected disks and planets around B9 to F5 type stars. Vertical lines show the cumulative mass of each planetary system, with dots highlighting planets from the most massive at bottom. Disk gas mass upper limits from HD lines are from this work (HD 163296) and from Kama et al. (2016b, HD 100546). For HD 163296, the range of CO-isotopolog based disk mass estimates is shown by a light blue bar (8×10^{-3} to 5.8×10^{-1} $M_\odot$; references in text). Also shown are the stellar mass divided by 10 and age; the mass limit for a gravitationally unstable disk (dashed line); an extrapolated dust-based disk mass range (dotted lines, Pascucci et al. 2016); and a population density colormap for planets around B9 to F5 type stars (data retrieved from `exoplanets.org` on 2019.07.16; bins contain from bottom to top 7, 6, and 1 planet). See text for individual planet and stellar mass references.

2018); at 145 au with 1.3 M_{Jup} (Liu et al. 2018; Teague et al. 2018); and at 260 au with 2 M_{Jup} (Pinte et al. 2018). Using the HD- and CO-based M_{gas} limits, and taking the combined mass of all published protoplanets in this disk as $\approx 5\,M_{Jup}$, we find the HD 163296 disk has converted 10 to 40 % of its mass into giant planets.

For HD 100546, the planet masses were constrained to be $\approx 10\,M_{Jup}$ at 10 au and $\sim 10\,M_{Jup}$ at 70 au by Pinilla et al. (2015). The mass of the outer planet could be $< 5\,M_{Jup}$ ($> 15\,M_{Jup}$) if it formed very early (late), so we adopt $10\,M_{Jup}$. The HD-based M_{gas} upper limit and the combined mass of the candidate planets yield a lower limit on the disk-to-planet mass conversion efficiency, $\gtrsim 30$ %.

Such high disk-to-planet mass conversion efficiencies combined with the presence of several gas giants per star raise the question of whether the planets formed through gravitational instability. Adding the M_{gas} upper limit and combined mass of proposed planets in either disk gives a result close to $0.1\,M_\odot$. This is approximately at the gravitationally unstable limit, so such a formation pathway may be feasible even with the current total mass in the system, although the local Toomre Q varies with radius and may leave the outer disk still far from instability (e.g. Booth et al. 2019).

We also show in Figure 6.7 three somewhat older stars of similar mass (HD 95086,

β Pic, and HR 8799) and their planets; standard disk mass estimates for stars of 1.5 and 3 $M_\odot$ based on $M_{\rm dust}$ relations from Pascucci et al. (2016) and scaled up with $\Delta_{\rm gd} = 100$; and a shaded log-scale histogram of the mass distribution of known planets around early-type stars[1]. Stellar masses are from the GAIA DR2 analysis by Vioque et al. (2018), and from David & Hillenbrand (2015, β Pic) and Stassun et al. (2018, HD 95086). Planet masses for individual systems are plotted as cumulative bars, with the highest-mass planet at the base. We compiled planet data from Teague et al. (2018), Pinte et al. (2018, 2019), Pinilla et al. (2015), Liu et al. (2018), Zhang et al. (2018), Rameau et al. (2013a,b), De Rosa et al. (2016), and Marois et al. (2008, 2010). Individual stellar masses are from Rhee et al. (2007), David & Hillenbrand (2015), Stassun et al. (2018), and Vioque et al. (2018).

The two HD-based disk $M_{\rm gas}$ limits in Fig. 6.7 exceed the combined mass of planets around HR 8799, the most massive known planetary system, by a factor of only three. The disk mass limits are also only a factor of three above combined mass of candidate protoplanets in the HD 100546 disk. Either A-type star disks can, in some cases, convert as much as 25 % or more of their mass into giant planets, or these planetary systems formed at a very early stage, perhaps while the central protostar and massive initial disk were still heavily accreting from the protostellar envelope in which they were embedded. The mass distribution of giant planets around main-sequence A and B stars (Fig. 6.7) is strongly skewed towards lower masses, suggesting that such extreme mass conversion events are either rare, or that the high-mass planetary systems are not stable on timescales beyond a few times 10 Myr.

6.5.2 Observing HD in Herbig disks with SOFIA/HIRMES, SPICA/SAFARI and emphOrigins Space Telescope

In the coming years, several facilities will or may become available for observing HD rotational lines. The HIRMES instrument for SOFIA is currently undergoing commissioning and is due to be delivered at the end of 2020 (Richards et al. 2018). HIRMES will have a high spectral resolution of R $\sim$ 100000, allowing us, for the first time to spectrally resolve the HD 1 - 0 line. The sensitivity of HIRMES will be similar to Herschel/PACS. Our models suggest some Herbig Ae/Be disks will be detectable with this instrument, assuming the necessary hours per source are available.

Figure 6.8 shows the detectability of our disk models with a 10 h SOFIA/HIRMES observation, assuming a distance of 150 pc. Of the flat models (group II disks), only the most massive ($M_{\rm gas} \sim 0.1\,M_\odot$) around stars with the highest stellar luminosity ($L_* \geq 50\,L_\odot$) are detectable. Among the flared models (group I), a larger fraction of disks is observable. All of the disk models $M_{\rm gas} = 0.1$ $M_\odot$ where $\Delta_{\rm gd} > 10$ should be detectable in 10 hrs with SOFIA/HIRMES. For those disks with $M_{\rm gas} = 0.01$ $M_\odot$, all systems with $L_* = 125$ $L_\odot$ and most systems with $L_* = 50$ $L_\odot$ are detectable. To maximize the chance of success, future SOFIA/HIRMES observations should select group I sources with high stellar luminosity.

Based on the stellar luminosities in Table 6.1 there are four group I sources that match these criteria best for SOFIA/HIRMES to detect the HD 1 – 0 line: HD 31293 (AB Aur), HD 100546, HD 179218 and HD 97048. For these sources a 10 h observation with SOFIA/HIRMES would improve the current upper limits by a factor 3–10 and constrain the gas-to-dust mass ratio to $\Delta_{\rm gd} \leq 50-100$ if the sources remain undetected.

[1]Planets retrieved from `exoplanets.org` on 2019.07.16.

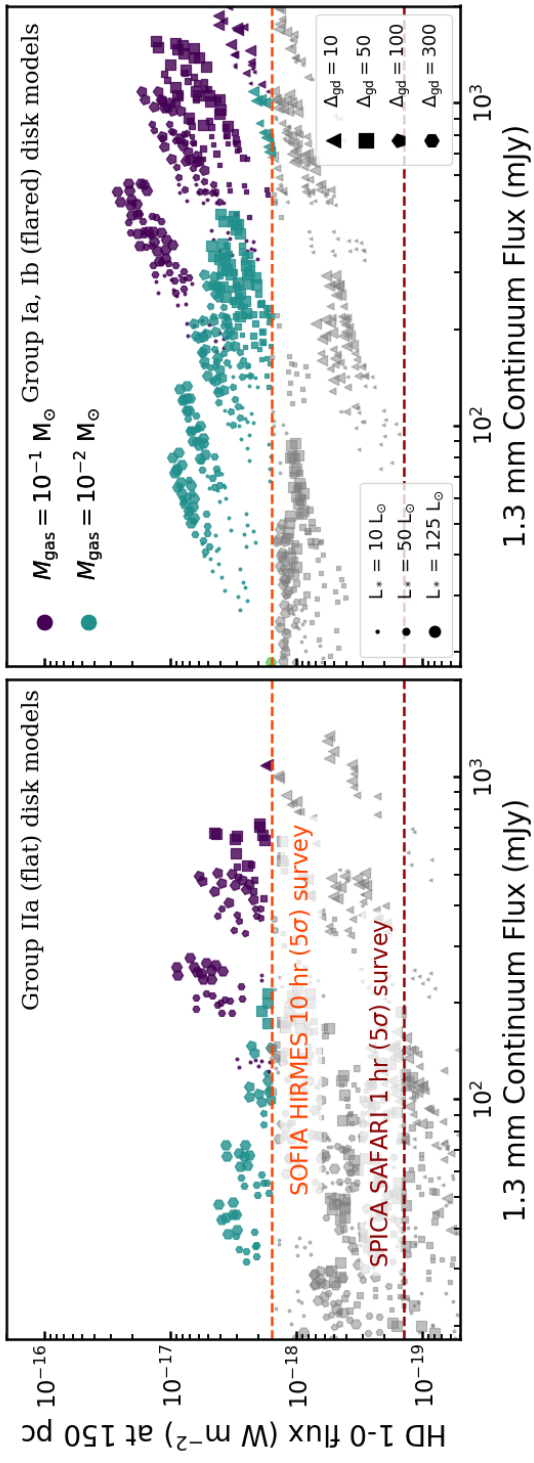

Figure 6.8: Observability of Group Ia,Ib (left) and Group IIa (right) models with SOFIA HIRMES. Colored disk models are detectable ($\geq 5\sigma$) with a 10 hr integration. Dark red dashed line shows the SPICA/SAFARI 1 hr detection limit. The *Origins Space Telescope* 1 hr detection limit ($\sim 1 \times 10^{-20}$ W m^{-2}) lies below the limits of the figure. Note that the fluxes are calculated for a distance of 150 pc.

Beyond SOFIA/HIRMES there are two proposed space missions focusing on far-infrared observations: SPICA/SAFARI and *Origin Space Telescope*. SPICA is one of the competitors for ESA's M5 opportunity, with a resolving power R $\sim$ 3000 and a 5σ 1 hr sensitivity of $1.3 \times 10^{-19}\,\mathrm{W\,m^{-2}}$ at $112\,\mu$m (Audley et al. 2018) . The *Origin Space Telescope* is a NASA mission concept. It would have high spectral resolution (R $\sim$ 43000) and sensitivity ($\sim 1 \times 10^{-20}\,\mathrm{W\,m^{-2}}$ in 1 hr) at $112\,\mu$m (Bonato et al. 2019). Hydrogen deuteride in all Herbig Ae/Be disks, and many T Tauris, within $\sim$ 200 pc will be detectable with these missions. However, both still require final approval and would only become available at the end of the 2020's at the earliest.

6.6 Conclusions

1. We find an overall gas mass upper limit of $M_{\mathrm{gas}} \leq 0.1\,\mathrm{M_\odot}$ is a strong conclusion for most of the disks studied. None of the disks are very likely to be strongly gravitationally unstable, although the constraints for HD 142527, HD 144668, HD 179218, and HD 31293 (AB Aur) are weak enough to allow for the possibility.

2. The HD 163296 disk mass is $M_{\mathrm{gas}} \leq 6.7 \times 10^{-2}\,\mathrm{M_\odot}$, based on the HD 1 – 0 upper limit. The CO-based literature lower limit is $M_{\mathrm{gas}} = 8 \times 10^{-3}\,\mathrm{M_\odot}$, contingent on the true level of gas-phase volatile depletion. The gas-to-dust ratio is thus $12 \leq \Delta_{\mathrm{gd}} \leq 100$, indicating gas dissipation may be proceeding faster than dust removal in this disk.

3. Comparing the HD 163296 and HD 100546 M_{gas} constraints with their proto-planet candidates and the HR 8799 giant planet system, we find that at least some Herbig Ae/Be disks convert the equivalent of $> 25\,\%$ of their present-day mass into giant planets.

4. Near-future SOFIA/HIRMES observations will probe the mass of flaring disks and large flat disks around A-type stars within ≈ 150 pc with $\gtrsim 10$ h integrations. SPICA/SAFARI will be crucial for larger sample studies of M_{gas} in disks. OST, if approved, would further revolutionise the field.

Appendix

6.A HD 1 - 0 fluxes for HD 135344B

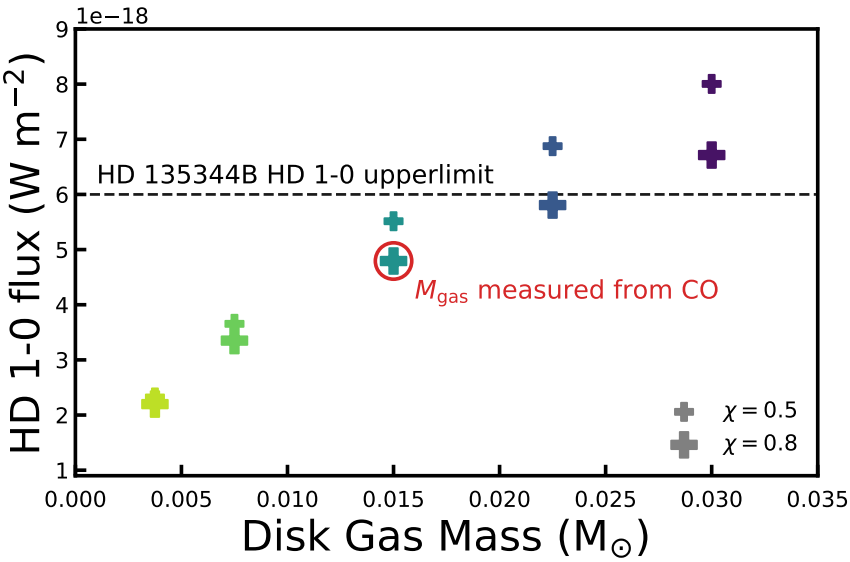

Figure 6.9: Comparing the HD135344B specific models from van der Marel et al. (2016b) to HD 1 - 0 upper limit (Fedele et al. 2013). All models have a dust mass $M_{\rm dust} = 1.3 \times 10^{-4}$ $M_\odot$ (cf. Table 3 in van der Marel et al. 2016b). The red circle shows the gas mass inferred from CO by van der Marel et al. (2016b).

Based on the HD135344B source-specific model from van der Marel et al. (2016a,b), we run a series of 10 models, varying the disk gas mass between 3.75×10^{-3} $M_\odot$ and 3×10^{-2} $M_\odot$. Figure 6.9 compares the HD 1 - 0 line fluxes of these models to the observed upper limit (Table 6.1). From the CO isotopolog observations van der Marel et al. (2016b) infer $M_{\rm gas} = 1.5 \times 10^{-2}$ $M_\odot$. This gas mass is in agreement with the gas mass upper limit inferred from HD 1 - 0, $M_{\rm gas} \leq 2.3 \times 10^{-2}$ $M_\odot$. Note that both gas masses are much lower than 0.1 $M_\odot$, making it highly unlikely that HD 135344B is gravitationally unstable (Section 6.4.6).

6.B HD 2-1 upper limits versus the model fluxes

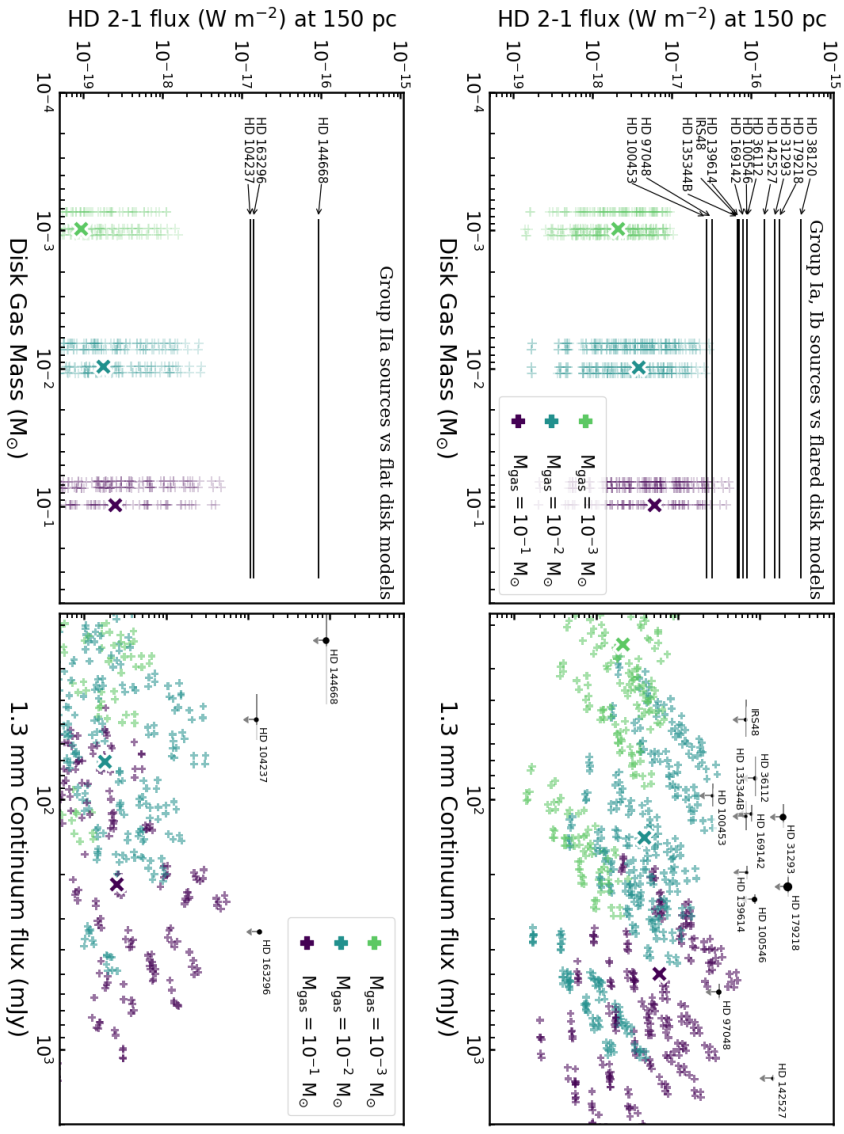

Figure 6.10: Upper limits on HD 56 μm line flux for the sample of Herbig Ae/Be disk systems (black lines) compared with our grid of DALI disk models (crosses). The top panels show the group I sources compared to models with flaring angle $\psi = 0.3$. The bottom panels show the group II sources compared to models with $\psi = 0.0$. **Left:** models are separated based on gas mass. **Right:** HD 2-1 upper limits set against 1.3 mm continuum fluxes for both observations and models.

6.C HD 1 - 0 line versus 1.3 mm continuum fluxes, showing gas-to-dust ratios and stellar luminosities

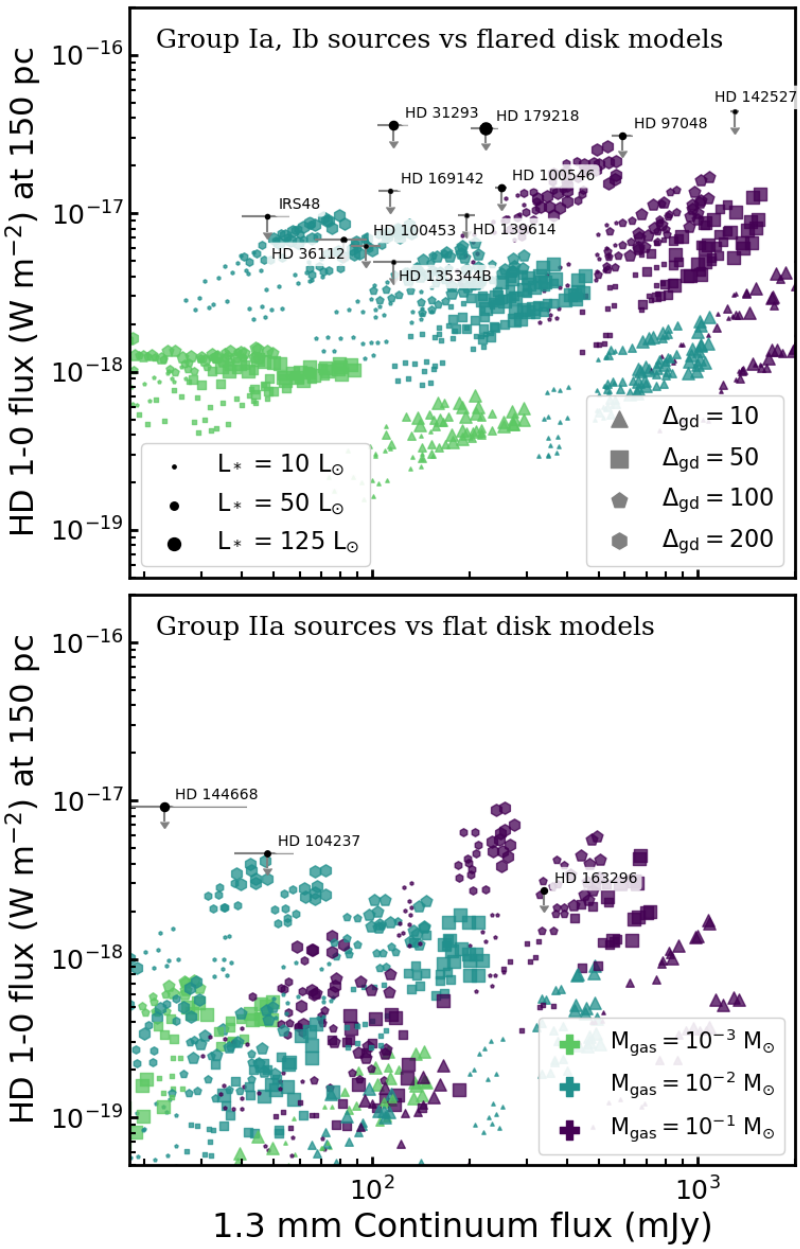

Figure 6.11: HD 1 - 0 line flux versus 1.3 continuum fluxes for both observations and models. Panels shown here are similar to right panels of Figure 6.3, but also showing the model gas-to-dust mass ratios (marker shape) and stellar luminosities (marker size).